Subramani, A., Maimí Vert, P., Guerrero Garcia, J.M., Costa i Balanzat, J. (2023). Nominal strength of notched pseudo-ductile specimens. Theoretical and Applied Fracture Mechanics, vol. 128, art. num. 104120. DOI https://doi.org/10.1016/j.tafmec.2023.104120

Graphical Abstract

Nominal strength of notched pseudo-ductile specimens

A. Subramani, P. Maimí, J. M. Guerrero, J. Costa

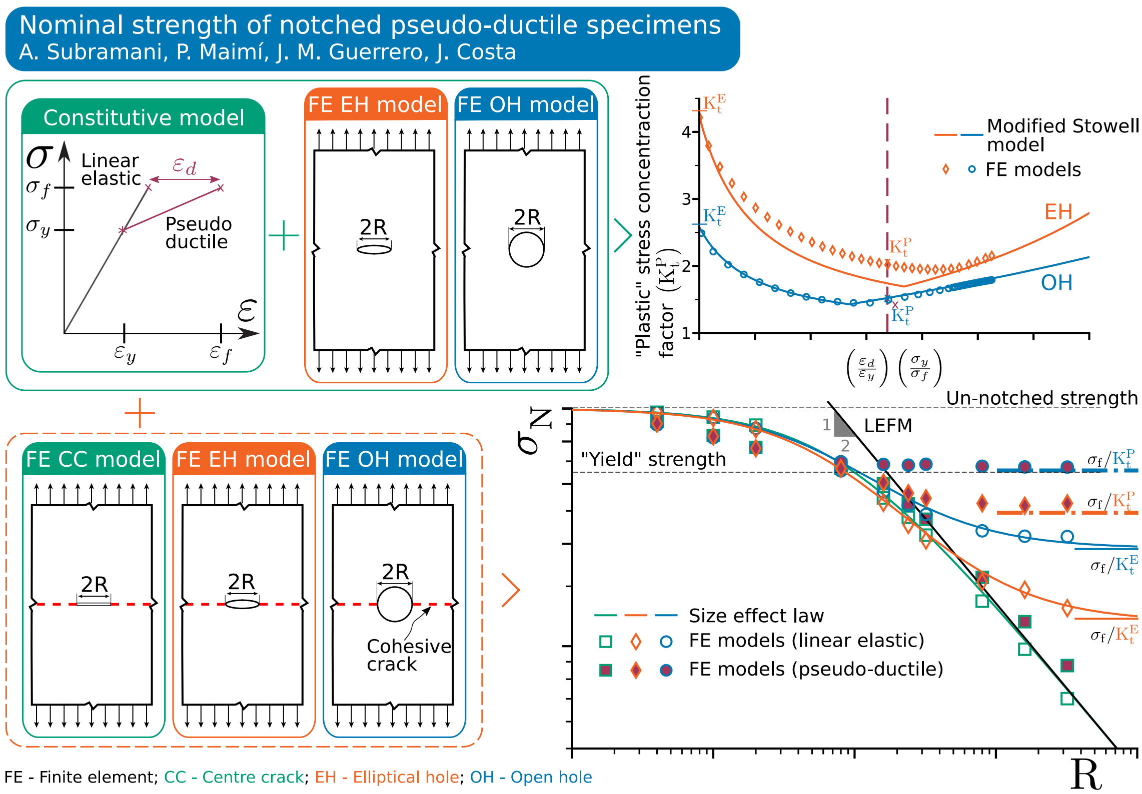

Highlights

Nominal strength of notched pseudo-ductile specimens

A. Subramani, P. Maimí, J. M. Guerrero, J. Costa

- Pseudo-ductility reduces stress concentration factor (K_t) by up to 50%.
- Increased nominal strength (σ_N) recovery of notched pseudo-ductile specimens due to reduced K_t.
- Closed form solution to determine pseudo-ductile K_t of elliptical and open hole specimens.

Nominal strength of notched pseudo-ductile specimens

A. Subramani, P. Maimí*, J. M. Guerrero, J. Costa

[a] *AMADE, Escola Politècnica Superior, Universitat de Girona, Girona, 17071, Spain*

Abstract

Quasi-brittle materials like composites are notch-sensitive, and the stress concentration factor (K_t) determines their strength knock-down. To alleviate this notch sensitivity, researchers are pursuing pseudo-ductility to stimulate stress redistribution around the notches. However, how such a pseudo-ductile material reduces K_t or improves the nominal strength (σ_N) in notched sub-components (centre crack, elliptical hole and open hole) is unclear. In this work, we analytically determine the K_t of typical notched specimens made of an idealised pseudo-ductile material and show its accuracy using Finite Element (FE) models. K_t increases after the specimen transitions from localised yielding to net-section yielding. Then, we elucidate the size-effect behaviour of the notched sub-components using FE models. The study reveals that the notched pseudo-ductile specimens recover higher σ_N than their linear elastic counterparts, in proportion to the K_t. However, pseudo-ductility decreases the σ_N for smaller specimens, and the notch shape is unimportant in this region.

Keywords: Stress concentration factor, Pseudo-ductility, Nominal strength, Numerical analysis, Analytical modeling

1. Introduction

Cut-outs, holes, and notches typically increase local stresses in a composite structure. Through the stress concentration factor (K_t), these stress intensifiers magnify the applied stress (σ) to $K_t\sigma$ in the notch vicinity. This results in a

*Corresponding authors
Email address: pere.maimi@udg.edu (P. Maimí)

structural response that falls between two extremes of notch sensitivity: "Totally notch in-sensitive" and "completely notch sensitive" (see Fig. 1). If the material is ideally plastic, the magnified stresses will be redistributed once the applied stress exceeds the plastic strength (σ_y), $\sigma > \sigma_y$, and this redistribution will cease only when the entire failure plane surrounding the notch plasticises. Conversely, if the material is brittle, the specimen will fail once the magnified stresses reach the material strength ($K_t\sigma = \sigma_f$).

In a notched material, plasticity reduces the stress concentration factor and, in consequence, the material retains more of the un-notched strength by moving the elastic limit line (σ_f/K_t) upward (Fig. 1). Though composite materials lack ductility, ply clustering (stacking plies of the same orientation together) leads to specimens with reduced notch sensitivity [1–3] thanks to stress relaxation from splitting (intralaminar cracks) and delaminations [1]. However, these large delaminations induce unacceptable nominal strength reduction, especially under compression and bending loads. The quest for thin ply laminates ($20 - 70$ µm per ply, which enhance un-notched strength and lesser manufacturing defects), exacerbates the issue of notch sensitivity due to their increased brittleness to stress concentrators [1, 4, 5]. Therefore, reducing notch sensitivity is highly desirable.

Pseudo-ductility features among the efforts to reduce the notch sensitivity of composite laminates and aims to introduce controlled sub-critical damage mechanisms that redistribute the magnified stresses [6–8]. Ply level hybridisation utilising thin-ply laminates – ply-by-ply stacks of alternating low and high ultimate strain lamina – is the typical way of achieving pseudo-ductile laminates [6, 9–12]. See Fig. 2 for the idealised stress-strain behaviour of such a pseudo-ductile uni-directional and quasi-isotropic laminate. Despite several studies on notched pseudo-ductile specimens [6, 9–11], its influence on the stress concentration factor is still unclear.

Nominal strengths of quasi-brittle materials are size-dependent, i.e., σ_N decreases when the specimens are scaled up for constant geometric ratios and material properties (Fig. 1). Though stress redistribution is expected to reduce the K_t across all specimen sizes, this effect is apparent only in larger specimens (Fig. 1). However, reduced notch sensitivity has been demonstrated experimentally only in smaller single-radius pseudo-ductile specimens, R=3 mm [10, 11, 13]. Furthermore, the nominal strength of single radius specimens is inadequate to characterise size-effect (σ_N from several different scaled notch radii are necessary). Thus, numerical models offer a way to characterise the impact pseudo-ductility has on the stress concentration factor and the nominal strength.

The objective of this work is to examine the impact pseudo-ductility has on the stress concentration factor and nominal strength of typical notches: Centre Crack (CC), Elliptical Hole (EH), and Open Hole (OH). The numerical analysis relies on a previously implemented user-material model by the same authors [14] representing pseudo-ductility. For completeness, we have a succinct overview of this model in Appendix A. We extend the existing analytical K_t estimates to incorporate pseudo-ductility (Neuber [15], Molski-Glinka [16] and Stowell [17]). In Section 4, we validate the K_t accounting for pseudo-ductility with FE simulations of EH and OH specimens. We use the FE models to determine the nominal strength of notched pseudo-ductile specimens considering the size effect (Section 5.2). Then, we summarise the impact pseudo-ductility has on nominal strengths by comparing the size-effect behaviour of linear elastic and pseudo-ductile materials for all three notches (Section 5.2.3). The estimated K_t provides the nominal strength limits. Finally, we compare stress distribution at peak load across the failure plane for small and large specimens of all three notches for a pseudo-ductile material (Section 5.2.4).

2. Size effect of notched quasi-brittle materials

Due to the presence of holes or cut-outs, there is a ductile to brittle failure mode transition depending on the specimen size (Fig. 1). This embrittlement resulting from the specimen size increase is attributed to the change in relative length of the Fracture Process Zone, ℓ_{FPZ}, to specimen size (notch radius,

R), ℓ_{FPZ}/R. The material's characteristic length (ℓ_M) introduced by Irwin [18] greatly captures ℓ_{FPZ} ($\ell_M \propto \ell_{FPZ}$). The Irwin length, ℓ_M, is a material property relating translaminar fracture toughness ($\mathcal{G}_{Ic}$), elastic modulus (E), and the ultimate strength (σ_f). If the stress perturbation caused by the notch is small with respect to the ℓ_{FPZ} (or cohesive zone), as in extremely small specimens ($R \to 0$), plastic collapse is expected and the nominal strength tends to material strength ($\sigma_N \to \sigma_f$, un-notched strength line in Fig. 1). On the other extreme, if stress perturbation is large in comparison to the ℓ_{FPZ}, as in very large specimens ($R \to \infty$), brittle failure is expected. This elastic limit (Fig. 1) corresponds to σ_f/K_t except for sharp notches. The size effect, σ_N vs ℓ_{FPZ}/R, for a geometrically similar structure results from asymptotically matching the elastic limit and the un-notched strength. The nominal strength is the ratio of the peak load, F_u, to the net-section area, $2(W-R)t$, given by,

$$\sigma_N = \frac{F_u}{2(W-R)t} \tag{1}$$

where W and t are specimen width and thickness, respectively. The nominal strength (σ_N) of any notched structure, normalised by the un-notched material strength (σ_f), is [19, 20]:

$$\begin{aligned} s_N = \frac{\sigma_N}{\sigma_f} &= \left(\frac{K_t^{-r} + \bar{\ell}_{\mathrm{SEL}}}{1+\bar{\ell}_{\mathrm{SEL}}}\right)^{\left(\frac{1}{r}\right)} \\ \bar{\ell}_{\mathrm{SEL}} = \frac{\ell_{\mathrm{SEL}}}{R} &= \frac{\ell_M}{RF^2} = \frac{E\mathcal{G}_{Ic}}{RF^2\sigma_f^2} \\ r &= 2\left[1-\left(\frac{1}{K_t}\right)\right] \end{aligned} \tag{2}$$

where $\bar{\ell}_{SEL}(=\ell_{FPZ}/RF^2)$ is the normalised ℓ_{FPZ} accounting for the finite width geometric correction factor, $\ell_{FPZ} = E\mathcal{G}_{Ic}/\sigma_f^2$. The parameter, r, is a fitting parameter. Since the s_N of the cracked specimens must also agree with Linear Elastic Fracture Mechanics (LEFM) when $R \to \infty$, r is defined as a function of K_t (as r should be 2 in the elastic limit, when $K_t \to \infty$). F is given by [21],

$$F = \left[1 - 0.025\left(\frac{R}{W}\right)^2 + 0.06\left(\frac{R}{W}\right)^4\right]\sqrt{\sec\left(\frac{\pi R}{2W}\right)} \tag{3}$$

3. Methodology

3.1. Numerical characterisation of pseudo-ductility

Pseudo-ductility is typically achieved by sandwiching low strain (LS) plies between high strain (HS) plies in the same orientation (ply-blocking) [6, 9, 22], see Fig. 2b, for example, glass-carbon-glass. Under uniaxial loading, the LS plies fragment and delaminate from these fragment ends. Once fragmentation and delamination saturate, the residual stiffness primarily originates from the high strain (HS) plies, resulting in a stress-strain response mimicking that of metals, Fig. 2a. To achieve quasi-isotropic stiffness with pseudo-ductile behaviour, these unidirectional (sub)laminates are stacked in desired orientations [9–11, 23], see Fig. 2 for the stress-strain response. The resulting uniaxial stress-strain response of such a quasi-isotropic laminate is shown in Fig. 2a. Indeed, the experimental response lacks the plateau region [9–11, 23, 24].

We opted for a macro-scale model at the laminate level to characterise the quasi-isotropic pseudo-ductile behaviour. Accordingly, the entire laminate is treated as an equivalent homogeneous material [25] and only the stress-strain response is necessary for our purposes. Further, this approach enables a rapid evaluation of various pseudo-ductile materials without being hindered by the subjacent intricacies. For example, several parameters, such as the relative thickness, thickness, modulus, strength, and failure strain ratios of the LS to HS materials, and interlaminar toughness, must all work in harmony to achieve pseudo-ductility. However, macro-scale approaches can only capture the sub-critical damage mechanisms that contribute to pseudo-ductility through changes in stiffness, not its underlying mechanisms.

We created a custom material subroutine to characterise the quasi-isotropic pseudo-ductility – elastic linear-“plastic” behaviour – under plane-stress loading with only in-plane damage mechanisms (see Figs. 2 and 3). For a detailed description of the material model, refer to Appendix A and Subramani et al., [14]. In brief, the failure surface is determined by the principal strain criterion, and the principal directions are fixed at the damage onset. In the elastic regime, the slope is defined by E, while after yielding ($\varepsilon > \varepsilon_y$, pseudo-ductile regime), a reduced slope of hE ($0 < h < 1$) is assumed until failure strength is reached. During unloading in the pseudo-ductile regime ($\varepsilon_y < \varepsilon < \varepsilon_f$), the response can be traced back to the origin with slope $m_i E$, where m_i is initially set to 1 to represent the integrity. It is not necessary to implement material softening after failure initiation ($\varepsilon > \varepsilon_f$) since we set the ultimate material strength to be equal to the cohesive traction strength ($\sigma_f = \sigma_c$). Thus, the crack will be forced to propagate in the *a priori* crack path, as illustrated in Fig. 4.

3.2. Non-dimensional analysis and design of experiments

The nominal strength – or the nominal stress concentration factor – of any notched structure is a function of both geometric and material parameters [19, 26, 27]. σ_N can be adequately characterised by,

$$\sigma_N = f\left(E, \sigma_y, \varepsilon_d, \sigma_f, \mathcal{G}_{Ic}, R, W, b\right) \tag{4}$$

where b is the semi-minor notch radius (y-direction in Fig. 4).

Using principles of dimensional analysis [28, 29], Eq. 4 can be rewritten as $p - q$ dimensionless parameters, where p and q are the number of independent variables ($p = 8$) and the number of primary dimensions, respectively. Considering, force, N, and length, L, as primary dimensions ($q = 2$), we have six non-dimensional variables, accordingly,

$$\frac{\sigma_N}{\sigma_f} = f_u\left(\varepsilon_y, \varepsilon_d, \frac{\sigma_f}{\sigma_y}, \frac{E\mathcal{G}_{Ic}}{R\sigma_f^2}, \frac{R}{W}, \frac{b}{R}\right) \tag{5}$$

Owing to many variables, we further simplify Eq. 5. We have numerically verified the insignificance of the pseudo-yield strain, ε_y, so we exclude it; as has also been done by others in [14, 30, 31]. Secondly, we assume a constant half-notch radius-to-width ratio (R/W) of 1/6 for all geometries. Rigorously, the laminate thickness, t, must also be included in Eq. 4, but we exclude it by assuming a unit thickness. Thus, Eq. 5 results in:

$$\frac{\sigma_N}{\sigma_f} = f_{u^*}\left(\varepsilon_d, \frac{\sigma_f}{\sigma_y}, \frac{E\mathcal{G}_{Ic}}{R\sigma_f^2}, \frac{b}{R}\right) \tag{6}$$

Through the "one-factor-at-a-time" approach, we first consider varying the material's non-dimensional groups: ε_d and $\sigma_f/\sigma_y(= s_H)$, as we did in [14]. In brief, we consider two studies (see Fig. 5): ε_{di} study (constant $s_H = 1.6$) and s_{Hi} study (constant $\varepsilon_d = 6.75\%$). Typical quasi-isotropic pseudo-ductile laminate properties were considered in both studies, $E_1 = E_2 = 25$ GPa (e.g., glass-carbon-glass quasi-isotropic laminate [11]) and a pseudo-yield strain of 1.25% ($\sigma_y = 312.5$ MPa). Further, ε_{di} took the values of 0.75%, 1.75%, and 6.75% (h = 0.5, 0.3, and 0.1) in the ε_{di} study, Fig. 5a. In the s_{Hi} study, we considered five strength ratios (s_H) ranging from 1.075 to 2, Fig. 5b. We included a pure linear-elastic case ($\varepsilon_d = 0, \varepsilon_y = \varepsilon_f = 2\%, \sigma_f = 500.0$ MPa) to validate and benchmark the FE models.

Nominal strengths are notch shape-dependent [19, 26, 27], b/R, in Eq. 6. We selected three different ratios of b/R ($\approx$0, 0.5, and 1), to represent CC, EH, and OH geometries, respectively, Fig. 4. In Eq. 6, we investigate size dependency, $E\mathcal{G}_{Ic}/R\sigma_f^2$, by increasing the half-notch size, R, from 0.2 to 160 mm (10 different R). For EH, we considered only an elastic and a pseudo-ductile material for all the notch sizes. While the length-to-width ratio does not affect the nominal strength (Eq. 6), one must avoid potential edge effects along the length direction. Given the computational cost of larger specimens, we selected a variable length-to-width ratio but ensured a minimum of $1.6W$, consistent with Xu et al. [32].

3.3. FE Models

We used the CC, EH and OH models to extract the nominal strength (or the peak load) for each specimen size and material. We maintained a constant translaminar fracture toughness, $\mathcal{G}_{Ic}$, of 75 $\mathrm{N\,mm^{-1}}$ in the cohesive elements for all the models. We utilised the linear traction-separation-based cohesive elements (COH2D4) available in Abaqus (version 6.14) to represent the crack. The constitutive model presented in Appendix A and in [14] were used in the continuum plane-stress (CPS4) elements with the corresponding material properties. We used an implicit solver with direct integration available in

Abaqus/Standard (*DYNAMIC, APPLICATION=TRANSIENT FIDELITY) due to the non-linear dynamic nature of the strength analysis and created two-dimensional, half-symmetric plane-stress models for each notch shape and notch radius, R, ranging from 0.2 to 160 mm. The FE models and their associated boundary conditions are shown in Fig. 4. Different meshes are created for each specimen width. The cohesive zone size ($\ell_{FPZ} = E\mathcal{G}_{Ic}/\sigma_f^2$), stemming from material softening, determines the element size. We ensure adequate cohesive elements in the softening region [33]. Using these element sizes, we verified mesh convergence in the models without pseudo-ductility, then scaled them based on specific pseudo-ductile material properties ($\mathcal{G}_{Ic}$ and σ_f). Elements also have a two-way bias (from the notch) towards both edges to minimise the element count.

Finite element models allow the stress concentration factor (K_t) and the elastic limit of notched specimens to be determined (Fig. 1). Furthermore, they permit the validation of the analytical K_t models [15, 16] accounting for pseudo-ductility in Section 4. The pseudo-ductile K_t (K_t^P) is determined using a single half-notch-radius specimen (R = 4 mm). In this case, we perform a linear elastic analysis by removing the cohesive elements in the FE models described above. We determine the K_t ($= \sigma_{max}/\sigma_{mean}$) by recording the notch tip stresses (σ_{max}) and the net mean stresses (σ_{mean}) from initial loading (zero stress) until material failure (σ_f) for the EH and OH models.

4. Stress concentration factor for pseudo-ductile materials

Commonly, the elastic strength limits (σ_f/K_t) of EH or OH specimens are determined using the K_t, given by handbooks such as [34], that assume the material to be elastic. Pseudo-ductile materials re-distribute stresses and, in consequence, lower the concentration factor. Therefore, we modify existing K_t models for metal plasticity (Neuber [15], Molski-Glinka [16] and Stowell [17]) to account for pseudo-ductility. The modified K_t^P can be represented by,

$$\left(K_t^P\right)_i = \frac{K_t^E}{\sqrt{1 + \Pi_i}} \tag{7}$$

where, the subscript i indicate N, for Neuber, and MG, for Molski-Glinka and K_t^E is the elastic stress concentration factor. With $e_d = \varepsilon_d/\varepsilon_y$, Π_N and Π_{MG} are given by,

$$\begin{aligned} \Pi_N &= \frac{e_d}{s_H} \\ \Pi_{MG} &= \frac{e_d}{s_H}\left(1+\frac{1}{s_H}\right) = \Pi_N\left(1+\frac{1}{s_H}\right) \end{aligned} \tag{8}$$

Both Neuber, $\left(K_t^P\right)_N$, and Molski-Glinka, $\left(K_t^P\right)_{MG}$, predict a monotonically decreasing K_t^P with e_d/s_H. However, K_t^P is expected to increase once the entire crack plane is nearly "plasticised" ($\sigma_{mean} > \sigma_y$), i.e., the average stress in the crack-plane is greater than the material yield strength. Thus, a better model is required to capture this phenomenon. The model of Stowell [17] captures it for a circular hole in an infinite plate. Later Herbert et al.,[35], generalised it to arbitrary notch configurations. The predictions of the Stowell model agreed well with the experiments for a wide range of notches/fillets [35] – even at deep 'plasticity". Therefore, we modify the Stowell model for an idealised pseudo-ductile material (Fig. 2) in detail below.

According to Stowell [17] and Herbert [35], the plastic stress concentration factor (K_t^P) for any notch is given by,

$$K_t^P = 1 + \left(K_t^E - 1\right)\frac{E_S\left(\sigma_{max}\right)}{E_S\left(\sigma_{mean}\right)} \tag{9}$$

where, $E_S(\sigma_{max})$ is the secant modulus of the material at the point of maximum stress, i.e., crack-tip, and $E_S(\sigma_{mean})$ is the secant modulus corresponding to the average stress in the failure plane, σ_{mean}. The adaptation to pseudo-ductility is straightforward, see Appendix B, and the final form of the K_t^P is given by:

$${K_t}^P = \begin{cases} {K_t}^E & \text{if } \sigma_{max} < \sigma_y \\ \frac{K_t^E + \Pi_N}{1+\Pi_N} & \text{if } \sigma_{max} > \sigma_y \text{ and } \sigma_{mean} < \sigma_y \\ \frac{K_t^E - 1 + h(1+\Pi_N)}{1+\left(K_t^E - 2\right)(1-h(1+\Pi_N))} & \text{if } \sigma_{mean} > \sigma_y \end{cases} \tag{10}$$

5. Results

5.1. Effect of pseudo-ductility on the stress concentration factor

To validate the pseudo-ductile stress concentration factor analytical models, we compared their evolution (Eq. 7 and Eq. 10 for EH and OH for the case of ε_{d4}), from yielding onset to material failure ($\varepsilon_y < \varepsilon < \varepsilon_f$) with FE solutions. The elastic stress concentration factor (K_t^E) for EH ($b/R = 1/2, R/W = 1/6$, Fig. 4) and OH ($R/W = 1/6$) are 4.24 and 2.58, respectively [34]. The K_t^E obtained with the linear-elastic FE models (ε_{d1}) agree within 0.5% of the handbook solutions for both the notches, thus validating the chosen approach.

The FE models display a pseudo-ductile K_t (K_t^P) behaviour similar to that of an elastic-plastic material [36], as seen in Fig. 6. The K_t^P decreases from K_t^E until the entire failure plane "plasticised" and then increases. Only the Stowell model (Eq. 10) captures such behaviour. Regardless of the notch shape, Neuber (Eq. 7) is in good agreement with the FE predictions under small-scale yielding conditions, while Molski-Glinka (Eq. 7) over-predicts for both notches.

The agreement of the Neuber model (Eq. 7) with the FE solutions depends on the notch shape. As Neuber modelled the notches as hyperbolic contours for mathematical simplicity, the agreement range with the FE solutions decreases from an e_d/s_H of 3.5 for an EH to 2 for an OH, see Fig. 6. On the other hand, the Molski-Glinka solutions agree only for very small $e_d/s_H (< 1)$ regardless of the notch geometry. The solutions of Stowell (Eq. 10) agree well with the FE solution for the entire range of e_d/s_H, especially for the OH. Comparing at the specific e_d/s_H (3.375) of the selected pseudo-ductile material (ε_{d4}), Stowell K_t^P (1.51) is within 0.6% of the FE solution (1.52), whereas Neuber (1.23) and Molski-Glinka (1.01) underpredict by 19 and 33%, respectively for an OH. On the other hand, for an EH, at the same e_d/s_H, Neuber (2.02) predicts within 0.5% of the FE (2.03) solution, whereas Stowell (1.74) and Molski-Glinka (1.66) underpredict by 14 and 18%, respectively.

To further corroborate the Stowell model (Eq. 10), and later calculate the elastic limit of σ_N, we obtained the OH pseudo-ductile K_t (K_t^P) using finite element (FE) models for all cases in the design of experiments, DOE (Fig. 5). Fig. 7 demonstrates that the Stowell predictions are in good agreement with the FE models for the entire range of e_d/s_H and for all the DOE in Fig. 5. The only deviation occurs in the case of s_{H1} ($s_H = 1.075, \varepsilon_d = 6.75\%$), where the Stowell solution slightly overestimates the FE solution by 5% at worst. The significant markers in the figure represent the exact e_d/s_H of the corresponding cases in Fig. 5. Thus, the Stowell model (Eq. 10) can be reliably used to determine the K_t^P of any pseudo-ductile material represented by the behaviour shown in Fig. 3b.

Furthermore, we expect the presented K_t^P responses to be general, as the fracture process is characterised by the significant non-dimensional parameters (Eq. 5). By carrying out the same process outlined in Section 4, we illustrate this generality, see Appendix C. The Stowell model (Eq. 10), correlates well with a coefficient of determination (R^2) of 0.87 and 0.99 for EH and OH cases, respectively (See Fig. C.11).

The Stowell model's success in Figs. 6 and 7 suggests that it can be adapted to other material behaviours. We validate this by extending it to the standard plasticity model (Ramberg-Osgood power law) typical of metals [37] and verifying it with Chen et al.'s [38] results in Appendix D.

5.2. Effect of pseudo-ductility on the nominal strength

Un-notched strength ($\sigma_N \to \sigma_f$) represents the maximum possible nominal strength, when $R \to 0$, independent of the notch shape. However, the minimum possible nominal strength is notch shape dependent: LEFM limit for sharp notches (CC), $\sqrt{\ell_M/(\pi F^2)}$, or elastic limit, σ_f/K_t, for other notch shapes (EH or OH) when $R \to \infty$.

We had observed pseudo-ductility to enhance the translaminar toughness [14]. With half-symmetric compact tension specimens (similar to [39]) and the pseudo-ductile constitutive model (refer to Appendix A and [14]), paired with a constant translaminar toughness ($\mathcal{G}_{Ic}$), we used the J-integral to capture this toughness increment. To avoid ambiguity; translaminar toughnesses are represented by $\mathcal{G}_{Ic}$ and $\mathcal{J}^{SS}$ for linear elastic and pseudo-ductile material, respectively. Thus, it is necessary to replace the linear elastic material fracture toughness ($\mathcal{G}_{Ic}$) with the pseudo-ductile material fracture toughness ($\mathcal{J}^{SS}$) for the size-effect predictions, refer to [14].

Previously, in [14], we had conducted a size effect study of pseudo-ductile CC specimens for the same material DOE as Fig. 5 following Section 3. Here, we use only the specific σ_N results (ε_{d1} and ε_{d4} studies) for comparison with other notch shapes (Section 5.2.3).

5.2.1. Nominal strength of open-hole specimens

The nominal strengths of the OH linear elastic models (ε_{d1}) agree well with the Bažant SEL Eq. 2, thus validating the models, Fig. 8a. Moreover, all the size-effect behaviour presented in Fig. 8, for all the DOE cases (Fig. 5), tend to both the un-notched strength and the elastic limit extremes set by the notch radius.

Significant improvements in strength recovery were observed for the large OH specimens (in proportion to pseudo-ductility), thanks to the improvements in both K_t and $\mathcal{G}_{Ic}$. The improvements in $\mathcal{G}_{Ic}$ are thought to have little influence on the nominal strengths of large OH specimens [27], while the reduction of K_t due to pseudo-ductility plays a significant role. For example, in the case of ε_{d4} (σ_f=500 MPa), a 41% reduction of K_t (from 2.58 to 1.52) leads to an improvement over the elastic strength of 60% for $2R$=320 mm, i.e., from 210 to 336 MPa, Fig. 8a. In other words, the largest pseudo-ductile (ε_{d4}) specimen lost only 33% (1 - 336/500) of material strength due to the presence of the notch ($1-s_N$), whereas the linear elastic specimen (ε_{d1}) lost 58% (1 - 210/500) of σ_f. Though, pseudo-ductility appears to negatively influence the nominal strengths by up to 14% in small specimens, the improvements in the large specimens outweigh this.

The nominal strengths for the cases in s_{Hi} study also tend to material strength and elastic limit, respectively, as expected (Fig. 8b). The K_t^P of s_{Hi} cases are reduced by up to 50% for s_{H1} (from 2.58 to 1.26), but the K_t increases with the increasing s_H (from 1.26 to 1.73) – only a 33% reduction for s_{H5}. Even though the pseudo-ductile translaminar toughness is only marginally accentuated for the s_{H1} case (σ_f=336 MPa) – $\mathcal{J}^{SS} = 1.06\mathcal{G}_{Ic}$ – the 50% reduction in K_t results in a strength recovery that is two times higher, 130 MPa (σ_f/K_t^E) to 272 MPa (σ_N). Similar comparison for s_{H5} (σ_f=625 MPa) shows only a recovery of 1.5 times, 242 MPa (σ_f/K_t^E) to 365 MPa (σ_N), despite a 40% increase in translaminar toughness – $\mathcal{J}^{SS} = 1.41\mathcal{G}_{Ic}$. In other words, s_{H1} lost only 19% (1 - 272/336) of material strength due to the notch $(1 - s_N)$, whereas s_{H5} lost 42% (1 - 365/625) of the material strength for the largest specimen considered.

In summary, the nominal strength results from Fig. 8 corroborate that the reduction in K_t^P due to pseudo-ductility is a substantial contributing factor to the strength recovery in the OH specimens. To determine the elastic limit, we directly use the K_t^P from Stowell predictions (Eq. 10) as they are nearly equal to the FE models (within 5%), see Section 5.1. As such, by utilising the K_t^P from the Stowell model, the elastic limits of all the pseudo-ductile models are captured within an error of 6%. Chen et al., [38] also presented a similar nominal strength retention behaviour of OH specimens made of metallic foams (Ramberg-Osgood material) under plane-strain conditions.

5.2.2. Nominal strength of elliptical-holed specimens

We anticipate a similar nominal strength behaviour for pseudo-ductile specimens containing EH [19, 40], as this lies between the extremes of the previously considered notch shapes, CC [14] and OH (Section 5.2.1). Therefore, we only consider a linear elastic (ε_{d1}) and a pseudo-ductile case (ε_{d4}). Fig. 9 focuses on the size effect behaviour of EH (represented by orange diamond markers).

The linear elastic FE models (ε_{d1}) match well with the Bažant SEL over the entire range of radii considered and follow the well-established nominal strength limits. Additionally, the nominal strength (σ_N) of the elliptical-holed pseudo-ductile models (ε_{d4}) follows similar trends to that of the OH models (Section 5.2.1), with a positive effect for larger models due to a sharp reduction in K_t^P, and a negative influence for smaller models. As such, the σ_N of ε_{d4} is recovered by 103% in comparison to the linear elastic case ε_{d1}, from 129 MPa ($(\sigma_N)_{\varepsilon_{d1}}$) to 263 MPa ($(\sigma_N)_{\varepsilon_{d4}}$). In other words, the linear elastic specimen, $2R = 320$ mm, lost 74% of the material strength (1 - 129/500), whereas, the pseudo-ductile specimen lost only half of it (47%, 1 - 263/500). The predictions for the elastic limit were not as accurate as those for the OH models, with the Stowell model under-predicting the K_t^P by 18% compared to the FE models. The difference between the elastic limit predictions using the K_t^P from the FE model ($\sigma_f/2.03$) and the Stowell model ($\sigma_f/1.74$) was -7% (246/263) and 9% (287/263), respectively.

5.2.3. Size effect of pseudo-ductile materials containing typical notches

To assess the impact pseudo-ductility has on notched specimens, including size-effect, we compare the nominal strengths of linear elastic (ε_{d1}) and pseudo-ductile models (ε_{d4}), Fig. 9. The σ_N of all linear elastic specimens agree with the Bažant size effect law (solid lines in Fig. 9). Furthermore, the linear elastic (empty markers) and the pseudo-ductile models (filled markers) exhibit the typical behaviour of notched specimens (see Fig. 1), including un-notched strength for smaller specimens and elastic limit for larger specimens.

The elastic limit of notched specimens scales in inverse proportion to the stress concentration factor ($\sigma_N = K_t^{-1}$), with CC having the lowest nominal strength (σ_N) due to its highest K_t ($K_t \to \infty$), followed by EH ($K_t^E = 4.24$) and OH ($K_t^E = 2.58$). Because of the notch, the largest elastic specimen ($2R$=320 mm) loses 86, 74, and 58% (σ_N=70, 129, 210 MPa) of the material strength for CC, EH and OH, respectively, i.e., 1 - σ_N/σ_f. Incorporating pseudo-ductility recovers more strength in general, thanks to the reduction of K_t for EH and OH specimens, and due to the $\mathcal{J}^{SS}$ for the CC, Fig. 9. The nominal strengths for the identical ($2R = 320$ mm) pseudo-ductile specimens are 25, 103, and 60% (σ_N=87, 263, 336 MPa) – $(\sigma_N)_{\varepsilon_{d4}}/(\sigma_N)_{\varepsilon_{d1}} - 1$ – higher than their linear elastic counterpart for CC, EH and OH, respectively.

However, the nominal strengths of smaller specimens ($2R < E\mathcal{J}^{SS}/\sigma_y^2 F^2$) are negatively influenced by pseudo-ductility by up to 14%, see Fig. 9. In this region, the hole shape does not play a significant role ($2R \to 0$) due to "plasticity"-dominated failure mode, resulting in almost equal nominal strength regardless of the notch type, see Section 5.2.4. This suggests the existence of an intermediate asymptotic behaviour typical of plastic-hardening materials [41, 42].

5.2.4. Stress distribution across the failure plane of notched pseudo-ductile specimens.

The nominal strength response of a quasi-brittle material is determined by the relative size of the stress perturbation to the FPZ length (Fig. 1b). We represent the normalised normal stress in the failure plane (σ_{yy}/σ_f) of all the notches considered (Fig. 10) to compare the FPZ lengths. The fracture processs zone is the non-linear region surrounding the crack tip, which is the sum of the cohesive ($o-a$ in Fig. 10) and "plastic" zone ($a-b$ in Fig. 10) lengths, see Fig. 3. Note that, these stresses are obtained just before specimen failure ($\sigma \approx \sigma_N$).

Normal stress distribution in the failure plane is similar for all notches considered (for a given radius, $2R$=2 mm), shown in Fig. 10a. Similar stress distributions emphasise that the K_t ($= \sigma_f/\sigma_{mean}$) is independent of the notch shape, as the σ_{mean} is the average of the normal stress in the failure plane. This results in nominal strengths that are independent of the notch shape (Fig. 9) for a given radius in the intermediate region ($2R < E\mathcal{J}^{SS}/\sigma_y^2 F^2$).

The fracture processs zone ($o - b$ in Fig. 10a) spans most of the specimen width in the limit of zero specimen size (very small specimens) and hence the entire width must be "plasticised", leading to $\sigma_N \approx \sigma_f$. Whereas, ℓ_{FPZ} spans only a small fraction of the width as the specimen size increases. For example, considering an OH specimen, the FPZ spans the entire specimen width for $2R$=2 mm (Fig. 10a). In contrast, FPZ spans only 25% for $2R$=320 mm, Fig. 10b.

6. Discussion

A notched pseudo-ductile composite coupon exhibits two different scales of damage mechanisms. Firstly, splitting and delamination [4, 43], act on the scales of specimen width (as observed in conventional composite laminates). Secondly, additional damage mechanisms (like ply/fibre fragmentation and dispersed delamination from the fragment ends) act on a much smaller length scale [10, 11, 13], in the order of ℓ_{FPZ}. In this study, we intend to capture only this FPZ length scale damage mechanisms, which are responsible for pseudo-ductility through stiffness change. Given that pseudo-ductility is generally achieved by ply-blocking (clustered HS ply in LS plies), ply splitting and delamination will play a non-negligible role in the stress redistribution. Although notched strength predictions must include them, interlaminar and intralaminar damage requires computationally expensive and complex mesoscale models (for e.g., [44]) to be captured. Therefore, the stress concentration factor we have obtained for pseudo-ductile materials (Section 4) is a conservative estimate, i.e., actual K_t might even be lower.

There are two main hindrances to comparing the nominal strengths of pseudo-ductile laminates presented in the literature [10, 11, 13], related to the small size of the explored specimens. Firstly, the assumption $K_t = \sigma_f/\sigma_N$ is only valid when $\ell_{FPZ}/W \approx 0$, and this does not hold for small specimens (Fig. 10). In small pseudo-ductile specimens, the cohesive traction at the crack tip is relevant, so the experimental results should not be compared to the analytical expressions of K_t (Eqs. 8 and 10). Secondly, nominal strengths obtained from a single small specimen ($2R$=3 mm in [10, 11, 13]) are insufficient to reveal the influence pseudo-ductility has on size-effect.

Achieving a near perfectly-"plastic" pseudo-ductile material represents the optimum configuration ($s_H \approx 1$, $e_d \to \infty$) from a purely notched strength perspective. For instance, s_{H1} displays 50% less K_t (1.26) and two times better strength recovery than an equivalent linear elastic material. To achieve such a material, $(\varepsilon_f)_{HS}$ must be 4.4 times higher than $(\varepsilon_f)_{LS}$ together with the lowest possible σ_f difference ($s_H \approx 1$). Through mesoscale models, Jalalvand et al. [45] also presented a similar reduction in the K_t of pseudo-ductile materials (e_d=4, s_H=1) in an OH under plane stress conditions (K_t was extracted from 0° layer). However, achieving perfect plasticity in practice is not feasible, so one must attempt to maximise e_d and minimise s_H.

7. Conclusions

We have presented a numerical study to characterise the influence of pseudo-ductility on the stress concentration factor (K_t) and nominal strength (σ_N) of composite laminates with typical notches (CC, EH, and OH). We utilised a user-material model that represents pseudo-ductility implemented in an FE environment. We explored the effect of the most significant variables affecting pseudo-ductility: pseudo-ductile strain (ε_d) and the material strength-to-yield strength ratio (σ_f/σ_y).

Firstly, we determined the pseudo-ductile stress concentration factor, K_t^P, of EH and OH by modifying existing models (Neuber, Molski-Glinka, and Stowell) and validated them with FE results. Neuber and Molski-Glinka agree well in the small-scale "yielding" regime but predict a monotonic decrease in K_t^P. Only the Stowell model predicts the increase in K_t when the specimens transition to net-section "yielding". Our results indicate that the modified Stowell model agrees with the FE results, especially for OH specimens. The predictions correspond to FE within 5% across the e_d/s_H range. This suggests a clear potential of pseudo-ductility to decrease K_t by as much as 50% for both EH and OH specimens.

Next, from the FE models, we demonstrated that the pseudo-ductility enhances the stress recovery of notched specimens. Notably, at the elastic limit ($R \to \infty$), pseudo-ductile specimens experience a nominal strength recovery between 25% and 103% compared to their linear elastic counterparts in the CC, EH and OH specimens. The adapted Stowell model captures the elastic limits of EH and OH specimens within 6% and 9%, respectively. However, pseudo-ductility hinders σ_N in the intermediate region, where it is independent of the notch-shape.

Our study highlights two potential avenues for application. First, presented K_t modifications offer insights to refine the size-effect laws for pseudo-ductility. Pseudo-ductile damage, post-yield, could be depicted as a ratio of the secant to the elastic modulus. Validation of such modified size-effect laws could leverage the presented FE results. Additionally, the Stowell model may be crucial for determining K_t in pseudo-ductile materials, essential to define the large-scale asymptote in modified size effect laws.

Acknowledgements

The authors acknowledge the funding and support of Ministerio de Ciencia, Innovación y Universidades for the project *En pos de materiales compuestos de fibra larga híbridos, bio-basados y sostenibles para aplicaciones estructurales* (SUBHYCO) (PID2021-126989OB-I00). Anbazhagan Subramani acknowledges the financial support of the Universitat de Girona for INV309_2019 and would also like to thank Universitat de Girona and Santander Universidades for the financial resources provided through *Personal Investigador en formació* (IF_UDG), 2020. Open Access funding provided thanks to the CRUE-CSIC agreement with Elsevier. José M. Guerrero would like to acknowledge the funding from the post-doc grant Margarita Salas with reference REQ2021_A_15, financed by the Spanish 'Ministerio de Universidades' and the European Union - Next Generation EU.

References

[1] A. Arteiro, G. Catalanotti, J. Xavier, P. Camanho, Notched response of non-crimp fabric thin-ply laminates, Composites Science and Technology 79 (2013) 97–114.

[2] A. Arteiro, G. Catalanotti, J. Xavier, P. Linde, P. Camanho, A strategy to improve the structural performance of non-crimp fabric thin-ply laminates, Composite Structures 188 (2018) 438–449.

[3] C. Soutis, Compressive strength of composite laminates with an open hole: Effect of ply blocking, Journal of composite materials 47 (2013) 2503–2512.

[4] R. Amacher, J. Cugnoni, J. Botsis, L. Sorensen, W. Smith, C. Dransfeld, Thin ply composites: Experimental characterization and modeling of size-effects, Composites Science and Technology 101 (2014) 121–132.

[5] A. Arteiro, C. Furtado, G. Catalanotti, P. Linde, P. Camanho, Thin-ply polymer composite materials: A review, Composites Part A: Applied Science and Manufacturing 132 (2020) 105777.

[6] G. Czél, M. R. Wisnom, Demonstration of pseudo-ductility in high performance glass/epoxy composites by hybridisation with thin-ply carbon prepreg, Composites Part A: Applied Science and Manufacturing 52 (2013) 23–30.

[7] G. Czél, S. Pimenta, M. R. Wisnom, P. Robinson, Demonstration of pseudo-ductility in unidirectional discontinuous carbon fibre/epoxy prepreg composites, Composites Science and Technology 106 (2015) 110–119.

[8] M. R. Wisnom, G. Czél, Y. Swolfs, M. Jalalvand, L. Gorbatikh, I. Verpoest, Hybrid effects in thin ply carbon/glass unidirectional laminates: accurate experimental determination and prediction, Composites Part A: Applied Science and Manufacturing 88 (2016) 131–139.

[9] G. Czél, M. Jalalvand, M. R. Wisnom, Design and characterisation of advanced pseudo-ductile unidirectional thin-ply carbon/epoxy–glass/epoxy hybrid composites, Composite Structures 143 (2016) 362–370.

[10] M. Fotouhi, M. Jalalvand, M. R. Wisnom, High performance quasi-isotropic thin-ply carbon/glass hybrid composites with pseudo-ductile behaviour in all fibre orientations, Composites Science and Technology 152 (2017) 101–110.

[11] M. Fotouhi, M. Jalalvand, M. Saeedifar, B. Xiao, M. R. Wisnom, High performance quasi-isotropic thin-ply carbon/glass hybrid composites with pseudo-ductile behaviour loaded off-axis, Composite Structures 247 (2020) 112444.

[12] Y. Swolfs, I. Verpoest, L. Gorbatikh, Recent advances in fibre-hybrid composites: materials selection, opportunities and applications, International Materials Reviews 64 (2019) 181–215.

[13] G. Czél, M. Jalalvand, M. Fotouhi, M. L. Longana, O. J. Nixon-Pearson, M. R. Wisnom, Pseudo-ductility and reduced notch sensitivity in multi-directional all-carbon/epoxy thin-ply hybrid composites, Composites Part A: Applied Science and Manufacturing 104 (2018) 151–164.

[14] A. Subramani, P. Maimi, J. Costa, On how pseudo-ductility modifies the translaminar fracture toughness of composites and the nominal strength of centre-cracked specimens., Submitted to Composites Part A: Applied Science and Manufacturing (2023).

[15] H. Neuber, Theory of notch stresses: principles for exact calculation of strength with reference to structural form and material, volume 4547, US-AEC Office of Technical Information, 1961.

[16] K. Molski, G. Glinka, A method of elastic-plastic stress and strain calculation at a notch root, Materials Science and Engineering 50 (1981) 93–100.

[17] E. Z. Stowell, Stress and strain concentration at a circular hole in an infinite plate, National Advisory Committee for Aeronautics Washington, DC, 1950.

[18] G. R. Irwin, Analysis of stresses and strains near the end of a crack traversing a plate, ASME Journal of applied mechanics 24 (1957) 361–364.

[19] P. Maimí, E. V. González, N. Gascons, L. Ripoll, Size effect law and critical distance theories to predict the nominal strength of quasibrittle structures, Applied mechanics reviews 65 (2013).

[20] Z. P. Bažant, Scaling theory for quasibrittle structural failure, Proceedings of the National Academy of Sciences 101 (2004) 13400–13407.

[21] H. Tada, P. C. Paris, G. R. Irwin, The Stress Analysis of Cracks Handbook, Third Edition, ASME Press, 2000.

[22] M. Jalalvand, G. Czél, M. R. Wisnom, Numerical modelling of the damage modes in ud thin carbon/glass hybrid laminates, Composites Science and Technology 94 (2014) 39–47.

[23] M. Fotouhi, M. Jalalvand, M. R. Wisnom, Notch insensitive orientation-dispersed pseudo-ductile thin-ply carbon/glass hybrid laminates, Composites Part A: Applied Science and Manufacturing 110 (2018) 29–44.

[24] G. Czél, Development of bi-directional pseudo-ductile glass/carbon-epoxy hybrid composites for improved safety in structural applications, Composites Part B: Engineering (2021) 109546.

[25] E. J. Barbero, Finite element analysis of composite materials using Abaqus™, volume 2103, CRC press Boca Raton, 2013.

[26] Z. P. Bažant, Size effect on structural strength: a review, Archive of applied Mechanics 69 (1999) 703–725.

[27] P. Maimí, D. Trias, E. González, J. Renart, Nominal strength of quasi-brittle open hole specimens, Composites science and technology 72 (2012) 1203–1208.

[28] E. Buckingham, On physically similar systems; illustrations of the use of dimensional equations, Physical review 4 (1914) 345.

[29] G. I. Barenblatt, Dimensional analysis, CRC Press, 1987.

[30] V. Tvergaard, J. W. Hutchinson, The relation between crack growth resistance and fracture process parameters in elastic-plastic solids, Journal of the Mechanics and Physics of Solids 40 (1992) 1377–1397.

[31] W. Brocks, A. Cornec, I. Scheider, 3.03 - computational aspects of non-linear fracture mechanics, in: I. Milne, R. Ritchie, B. Karihaloo (Eds.), Comprehensive Structural Integrity, Pergamon, Oxford, 2003, pp. 127–209.

[32] X. Xu, M. R. Wisnom, Y. Mahadik, S. R. Hallett, An experimental investigation into size effects in quasi-isotropic carbon/epoxy laminates with sharp and blunt notches, Composites Science and Technology 100 (2014) 220–227.

[33] A. Turon, C. G. Davila, P. P. Camanho, J. Costa, An engineering solution for mesh size effects in the simulation of delamination using cohesive zone models, Engineering fracture mechanics 74 (2007) 1665–1682.

[34] W. D. Pilkey, D. F. Pilkey, Z. Bi, Peterson's stress concentration factors, John Wiley & Sons, 2020.

[35] F. Herbert, A study of elastic and plastic stress concentration factors due to notches and fillets in flat plates, Annual Report-National Advisory Committee for Aeronautics 103 (1955) 213.

[36] H. Hardrath, L. Ohman, A study of elastic and plastic stress concentration factors due to notches and fillets in flat plates, Technical Report, National Advisory Committee for Aeronautics, 1953.

[37] W. Ramberg, W. R. Osgood, Description of stress-strain curves by three parameters, NACA-TN-902, Technical Report, National Advisory Committee for Aeronautics, 1943. Available at https://ntrs.nasa.gov/citations/19930081614.

[38] C. Chen, N. A. Fleck, T. Lu, The mode i crack growth resistance of metallic foams, Journal of the Mechanics and Physics of Solids 49 (2001) 231–259.

[39] A. Ortega, P. Maimí, E. González, L. Ripoll, Compact tension specimen for orthotropic materials, Composites Part A: Applied Science and Manufacturing 63 (2014) 85–93.

[40] Z. P. Bažant, J. Planas, Fracture and size effect in concrete and other quasibrittle materials, Routledge, 2019.

[41] H. T. Nguyen, A. A. Dönmez, Z. P. Bažant, Structural strength scaling law for fracture of plastic-hardening metals and testing of fracture properties, Extreme Mechanics Letters 43 (2021) 101141.

[42] S. Morel, Size effect in quasibrittle fracture: derivation of the energetic size effect law from equivalent lefm and asymptotic analysis, International journal of fracture 154 (2008) 15–26.

[43] A. Arteiro, Structural mechanics of thin-ply laminated composites, Phd thesis, Universidade do Porto, Porto, Portugal, 2016. Available at https://hdl.handle.net/10216/83363.

[44] P. Maimí, P. P. Camanho, J. Mayugo, C. Dávila, A continuum damage model for composite laminates: Part i–constitutive model, Mechanics of materials 39 (2007) 897–908.

[45] M. Jalalvand, G. Czel, M. Wisnom, Reducing the notch sensitivity of quasi-isotropic layups using thin-ply hybrid laminates, in: X. Xiao, A. Loos, D. Liu (Eds.), Proceedings of the American Society for Composites - 30th Technical Conference, ACS 2015, American Society for Composites, 2015.

[46] P. Maimí Vert, Modelización constitutiva y computacional del daño y la fractura de materiales compuestos, Phd thesis, Universitat de Girona, Girona, Spain, 2007. Available at http://hdl.handle.net/10803/7766.

[47] J. E. Marsden, T. J. Hughes, Mathematical foundations of elasticity, Courier Corporation, 1994.

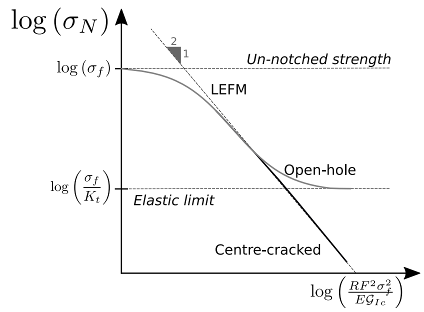

Figure 1: Size dependency of the nominal strength (σ_N) of quasi-brittle materials. Un-notched strength and elastic limit represent the totally notch insensitive and completely notch sensitive responses, respectively. $E\mathcal{G}_{Ic}/(R\sigma_f^2)$ is the normalised material characteristic length.

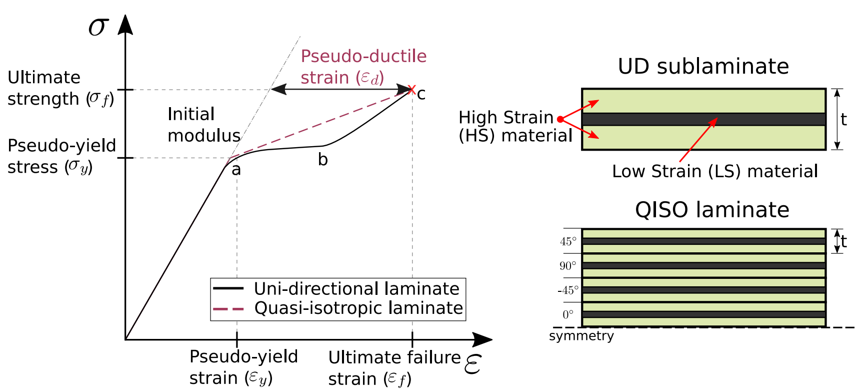

Figure 2: a) Idealised uni-axial tensile response of unidirectional (solid) and quasi-isotropic (dotted) pseudo-ductile composite laminates and b) Example of a typical pseudo-ductile unidirectional and quasi-isotropic laminate.

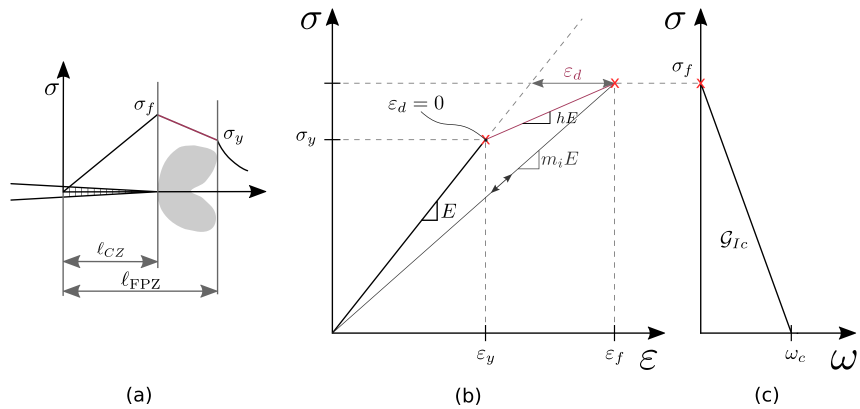

Figure 3: Description of a) fracture processs zone and associated lengths b) pseudo-ductile constitutive behaviour and c) traction-separation behaviour (Cohesive law).

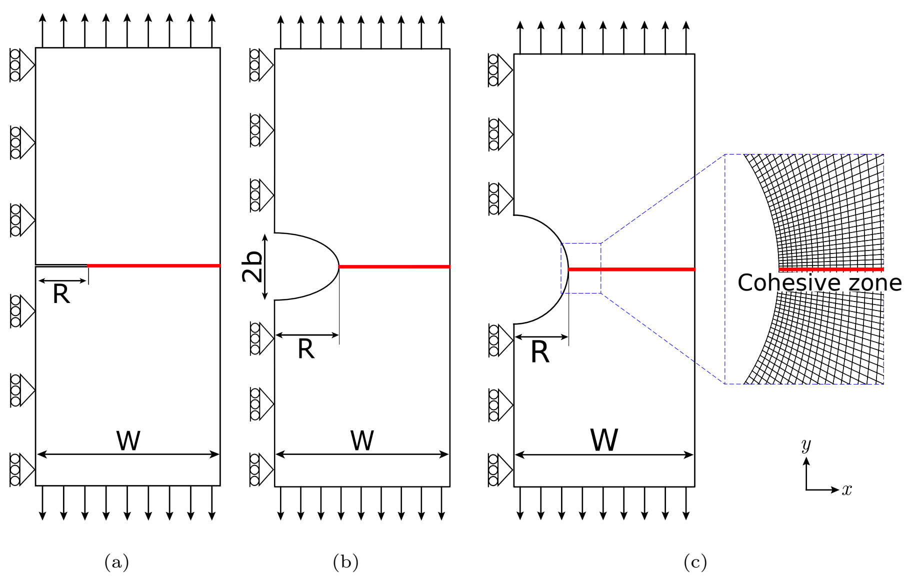

Figure 4: Representative half-symmetric FE models of (a) centre-crack, (b) elliptical hole and (c) open hole specimens and their boundary conditions. R and W are notch radius and specimen half-width respectively.

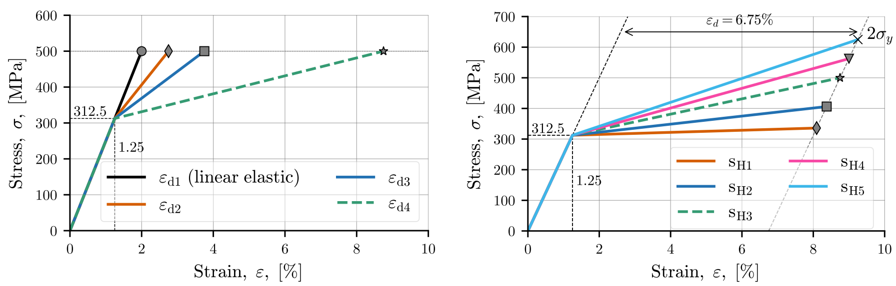

(a) (b)

Figure 5: Design of experiments for the quasi-isotropic pseudo-ductile material. (a) ε_{di} study with the constant non-dimensional variable s_H (=1.6) with ε_d values of 0, 0.75%, 1.75% and 6.75% and (b) s_{Hi} study with the constant non-dimensional variable ε_d (= 6.75%) with s_H values of 1.075, 1.3, 1.6, 1.8 and 2.0. Note that ε_{d4} and s_{H3} are equivalent.

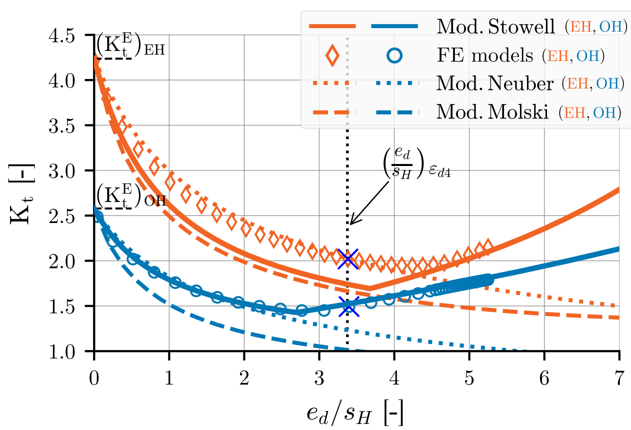

Figure 6: Comparison of the modified analytical stress concentration factor estimates to FE solution (markers) for a pseudo-ductile material (ε_{d4}). The analytical models are Neuber (dotted lines, Eqs. 7 and 8), Molski-Glinka (dashed lines, Eqs. 7 and 8) and Stowell (solid lines, Eq. 10). Note the cross marker (x) represents the e_d/s_H $\left((\varepsilon_d/\varepsilon_y)\left(\sigma_y/\sigma_f\right)\right)$ of ε_{d4} (e_d = 5.4, s_H=1.6) case. Here, e_d is the pseudo-ductile to "yield" strain ratio, while s_H denotes the un-notched to pseudo-yield strength ratio.

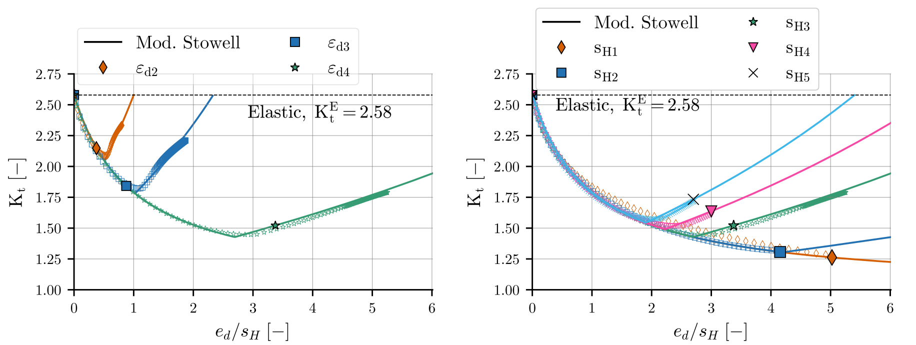

(a) (b)

Figure 7: Open-hole K_t determined by the modified Stowell model (Eq. 10) for (a) ε_{di} study, and (b) s_{Hi} study in Fig. 5 compared to FE results. Empty markers represent the FE results and the single filled marker represent the corresponding $e_d/s_H = (\varepsilon_d/\varepsilon_y)\left(\sigma_y/\sigma_f\right)$ of all cases selected for ε_{di} and s_{Hi} studies. Note that ε_{d4} and s_{H3} are equivalent. Here, e_d is the pseudo-ductile to "yield" strain ratio, while s_H denotes the un-notched to pseudo-yield strength ratio.

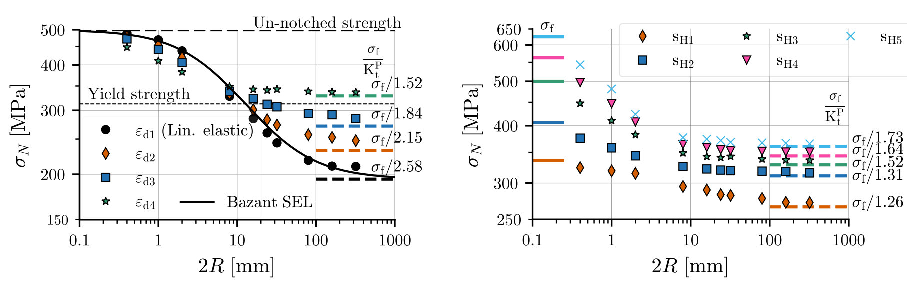

(a) (b)

Figure 8: Nominal strengths of the pseudo-ductile open-hole specimens in (a) ε_{di} study, and (b) s_{Hi} study in Fig. 5. The continuous solid line for the linear elastic material (ε_{d1}) is determined by the Bažant SEL (Eq. 2). The short dashed lines represent the elastic limit, σ_f/K_t^P, and the K_t^P is determined from modified Stowell Eq. 10. Note that the y-axis scales are different between (a) and (b).

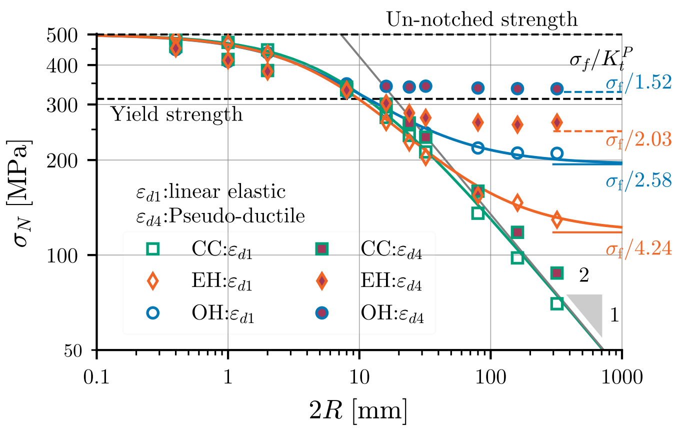

Figure 9: Nominal strength of centre-cracked (green squares), elliptical-hole (orange diamonds), and open-hole (blue circles) linear elastic (ε_{d1}, empty markers) and pseudo-ductile (ε_{d4}, filled markers) specimens. The continuous solid line for the linear elastic material is determined by the Bažant SEL (Eq. 2). Note that the elastic limit $\left(\sigma_f/K_t^P\right)$ here is determined with the K_t^P from the finite element models.

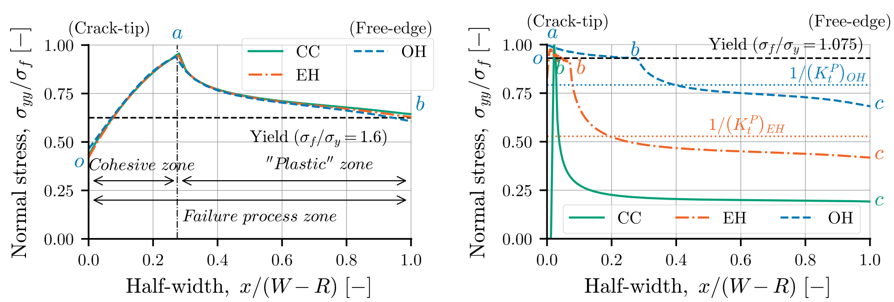

(a)

(b)

Figure 10: Normal stress distribution across the specimen width for pseudo-ductile centre-crack, elliptical-hole and open-hole specimens, (a) 2R = 2 mm with ε_{d4}, towards un-notched strength limit and (b) 2R = 320 mm with s_{H1}, towards elastic limit. Regions: $o-a$ represent length of the cohesive zone (ℓ_{cz}), $o-b$ represent the total fracture processs zone length (ℓ_{FPZ}) and $b-c$ represent the linear elastic zone.

Appendices

A. Constitutive model to characterise pseudo-ductility

Under isothermal conditions, the complementary Gibbs free energy density (Ψ) for an idealised quasi-isotropic pseudo-ductile laminate (as in Fig. 3b), following [46], is postulated as,

$$\Psi := \frac{1}{2E}\left(\frac{\sigma_{11}^2}{m_1} + \frac{\sigma_{22}^2}{m_2} - 2\nu\sigma_{11}\sigma_{22} + 2\sigma_{12}^2\left[\frac{1+\nu\sqrt{\mathrm{m}_1\ \mathrm{m}_2}}{\sqrt{\mathrm{m}_1\ \mathrm{m}_2}}\right]\right) \tag{A.1}$$

where E and ν are the elastic modulus and the poissons' ratio of the undamaged material, respectively. The integrity functions m_1 and m_2 start with a value of 1 and decreases with the degradation, accounting for potential anisotropy in damage evolution. Note that the shear modulus (G) is embedded within Eq. A.1, as $E\sqrt{m_1 m_2}/2(1+\nu\sqrt{m_1 m_2}) = G$. We can derive the strain tensor (ε) from Ψ using the Clausius-Duhem inequality [47], as,

$$\varepsilon = \frac{\partial\Psi}{\partial\sigma} = \mathbb{H}\sigma \quad \text{where:} \quad \mathbb{H} = \frac{1}{E}\begin{bmatrix} \frac{1}{m_1} & -\nu & 0 \\ -\nu & \frac{1}{m_2} & 0 \\ 0 & 0 & \frac{E}{G} \end{bmatrix} \tag{A.2}$$

where, $\mathbb{H}$ is the compliance tensor. The principal directions of damage are defined by two damage surfaces (longitudinal and transversal) using,

$$F_i = \sqrt{\langle\bar{\varepsilon}_{ii}\rangle^2 + \eta\bar{\varepsilon}_{12}^2} - \kappa_i - \varepsilon_y \leq 0 \quad \text{for } i = 1, 2 \tag{A.3}$$

where κ_1 and κ_2 are internal variables initialised to 0, and η represents the shear contribution set to 1 throughout. The integrity of the material point is determined by scalar damage variables (d_i), ranging from 0 (undamaged) to 1 (fully damaged), such that $m_i = 1 - d_i$. The functions F_i are calculated in the principal strain directions when there is no damage and later frozen in the damage direction. Thus, degradation initiates according to the maximum principal strain criterion. The model is then integrated as follows,

$$\kappa_i = \max_{s=0,t}\left\{\sqrt{<\bar{\varepsilon}_{ii}>^2 + \eta\bar{\varepsilon}_{12}^2}\right\} - \varepsilon_y \tag{A.4}$$

The integrity function is defined as:

$$m_i = \frac{H\left(\kappa_i + \varepsilon_y\right) + \sigma_y}{E\left(\kappa_i + \varepsilon_y\right)} \quad \text{if } \varepsilon_y < \kappa_i \tag{A.5}$$

where $H = \left(\sigma_f - \sigma_y\right) / \left(\varepsilon_f - \varepsilon_y\right)$ is the tangent modulus of the linear strain "hardening" region and $h = H/E$ is the "hardening" modulus ratio.

B. Modification of the Stowell stress concentration factor to account for pseudo-ductility

According to Stowell, the plastic K_t depends on the secant modulus ratio, $E_S(\sigma_{max})/E_S(\sigma_{mean})$. For the idealised pseudo-ductile material considered here (Fig. 2a), there exist three distinct regions of the secant modulus ratios, $E_S(\sigma_{max})/E_S(\sigma_{mean})$, and so the stress concentration factor. They are:

1. Completely elastic (no "yielding" anywhere): $\sigma_{max} < \sigma_y$,
2. Small-scale yielding (some "yielding" in the failure plane): $\sigma_{max} > \sigma_y$ and $\sigma_{mean} < \sigma_y$, and
3. Large-scale yielding (entire failure plane is "yielding"): $\sigma_{mean} > \sigma_y$

The failure stress, σ_f, for a quasi-isotropic pseudo-ductile material (see Fig. 2) can be expressed as,

$$\sigma_f = \left(\varepsilon_f - \varepsilon_y\right) H + \sigma_y \tag{B.1}$$

where H is the "hardening" modulus. We present three different forms of Eq. B.1 in terms of the non-dimensional material parameters, h, e_d and s_H to obtain simplified K_t^P:

$$\begin{aligned} h &= \frac{H}{E} = \frac{s_H - 1}{s_H - 1 + e_d} \\ e_d &= \frac{\varepsilon_d}{\varepsilon_y} = \frac{(1-h)\left(s_H - 1\right)}{h} \\ s_H &= \frac{\sigma_f}{\sigma_y} = 1 + \frac{h e_d}{1-h} = \frac{1-h}{1 - h - \left(\frac{h e_d}{s_H}\right)} \end{aligned} \tag{B.2}$$

With the above material relationships (Eq. B.2), the secant modulus, E_S, for any arbitrary stress (σ_k) in the "hardening" region ($\sigma_k > \sigma_y$) can be defined as,

$$E_S\left(\sigma_k\right) = \frac{\sigma_k}{\varepsilon_k} = \frac{\sigma_k}{\varepsilon_y + \left(\varepsilon_k - \varepsilon_y\right)} = \frac{\left(s_H - 1\right) E\sigma_k}{\sigma_k\left(s_H - 1 + e_d\right) - e_d\sigma_y} \tag{B.3}$$

We consider failure strength to be the maximum stress anywhere in the specimen, $\sigma_{max} = \sigma_f$, and the mean net stress across the failure plane to be the failure strength by ${K_t}^P$, $\sigma_{mean} = \sigma_f / K_t^P$. Substituting these assumptions and the secant modulus (Eq. B.3) to the respective regions presented earlier, elastic, small scale yielding (SSY) and large scale yielding (LSY), in Eq. 9, we can obtain the piecewise K_t^P for each regime,

$${K_t}^P = \begin{cases} {K_t}^E & \text{if } \sigma_{max} < \sigma_y \\ \frac{K_t^E + \Pi_N}{1 + \Pi_N} & \text{if } \sigma_{max} > \sigma_y \text{ and } \sigma_{mean} < \sigma_y \\ \frac{K_t^E - 1 + h(1 + \Pi_N)}{1 + \left(K_t^E - 2\right)(1 - h(1 + \Pi_N))} & \text{if } \sigma_{mean} > \sigma_y \end{cases} \tag{B.4}$$

C. Stress concentration factor of other pseudo-ductile materials

To verify the general applicability of the modified Stowell relations (Eq. 10), we conducted a complementary set of design-of-experiments similar to Section 3.2. Here, we considered three additional logarithmically increasing pseudo-ductile strains (0.5%, 1.2%, and 2.85%) with the same five strength ratios (ranging from 1.075 to 2), resulting in 20 additional pseudo-ductile materials. We recorded the pseudo-ductile stress concentration factor (K_t^P) for each material and notch (elliptical and open-hole) using the procedure outlined in Section 3.3. We present the results as a "1:1" plot of the K_t^P predicted by the Stowell model (Eq. 10) in comparison to the FE results, see Fig. C.11, with only a scalar K_t^P at the corresponding e_d/s_H of each pseudo-ductile material for clarity. The results show that the modified Stowell model (Eq. 10) works well for both EH and OH.

D. Stress concentration factor of power-law materials

The adaptation of stress concentration factor to the power-law materials is straightforward to the linear "hardening" plasticity presented earlier in Appendix B. Hence, only a brief description is provided here.

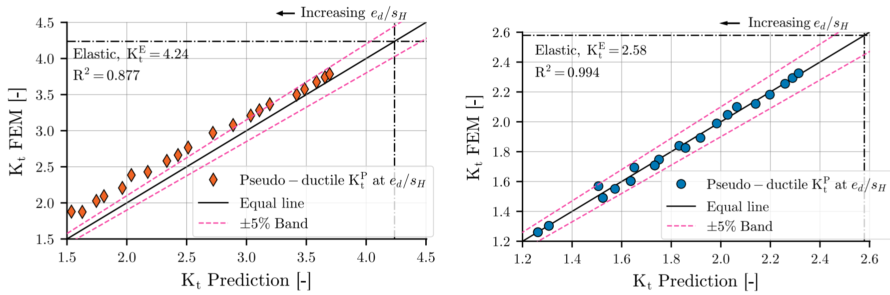

(a) (b)

Figure C.11: The "1:1" plot of pseudo-ductile stress concentration factor, comparison of FE solutions to modified Stowell relations (Eq. 10). a) Elliptical hole and b) Open-hole. Dash-dotted line represents the elastic K_t^E for the geometric configuration considered.

The standard plasticity model (Ramberg-Osgood) is represented by,

$$\varepsilon = \begin{cases} \frac{\sigma}{E} & \text{if } \sigma \leq \sigma_y \\ \varepsilon_y \left(\frac{\sigma}{\sigma_y}\right)^{1/N} & \text{if } \sigma > \sigma_y \end{cases} \tag{D.1}$$

The secant modulus (E_S) variation past yielding can be obtained by modifying Eq. D.1,

$$E_S(\sigma_k) = \frac{\sigma_k}{\varepsilon_k} = \frac{\sigma_k}{\varepsilon_y \left(\frac{\sigma_k}{\sigma_y}\right)^{(1/N)}} \tag{D.2}$$

Substituting the secant modulus (Eq. D.2) with Stowell K_t^P in Eq. 9 for the corresponding SSY and LSY conditions, results in:

$$K_t^P = 1 + \left(K_t^E - 1\right) s_H{}^{\left(\frac{N-1}{N}\right)} \text{ if } \sigma_{max} > \sigma_y \text{ and } \sigma_{mean} < \sigma_y \tag{D.3}$$

$$K_t^P \approx 1 + \left(K_t^E - 1\right) \left(\frac{1}{K_t^P}\right)^{\left(\frac{1-N}{N}\right)} \text{ if } \sigma_{max} > \sigma_y \text{ and } \sigma_{mean} > \sigma_y \tag{D.4}$$

In Fig. D.12, we depict $K_t(e_d/s_H)$. Although unconventional in standard plasticity models, this choice aligns with Figs. 6 and 7, it is defined by,

$$\frac{e_d}{s_H} = s_H{}^{\left(\frac{1}{N}-1\right)} - 1 \tag{D.5}$$

After the transition to large-scale yielding (LSY), solving the plastic stress concentration factor (Eq. D.4) requires an iterative approach. The solutions

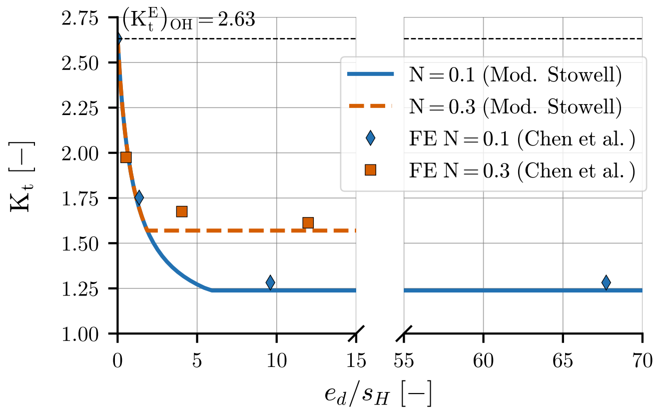

Figure D.12: K_t^P for a Ramberg-Osgood material obtained using Eqs. D.3 and D.4. Markers represent the finite element solution presented by Chen et al. [38]. Analytical elastic K_t of 2.63 for open-hole is used, provided by the same authors [38].

obtained using Eqs. D.3 and D.4 agree well with the finite element (FE) solutions from [38] for OH specimens, see Fig. D.12. Compared to linear "hardening" plasticity (Fig. 7), the notable feature of plastic K_t for power-law materials is that it is constant when $\sigma_{max} > \sigma_y$ and $\sigma_{\mathrm{mean}} > \sigma_{\mathrm{y}}$, which depends solely on the exponent N.